Reference Governor Based Solution for Satellite Attitude Control in Presence of Multiple Disturbances and Actuator Saturations

Guido Magnani, Jean-Marc Biannic, Mario Cassaro, Hélène Evain, Laurent Burlion

DOI: 10.13009/EUCASS2022-4473
9TH EUROPEAN CONFERENCE FOR AERONAUTICS AND SPACE SCIENCES (EUCASS)

Reference Governor Based Solution for Satellite Attitude Control in Presence of Multiple Disturbances and Actuator Saturations

MAGNANI Guido[⋆†], *BIANNIC Jean-Marc*[⋆], *CASSARO Mario*[⋆], *EVAIN Hélène*[¶] *and BURLION Laurent*[§]
[⋆]*ONERA, Toulouse, France (e-mail: name.surname@onera.fr)*
[¶]*CNES, Toulouse, France (e-mail: name.surname@cnes.fr)*
[§]*Rutgers University, New Brunswick, NJ, USA (e-mail: name.surname@rutgers.edu)*
[†]Corresponding author

Abstract

This paper deals with satellite attitude control in presence of propellant sloshing and flexible appendages disturbances. The control framework is based on a robust H_∞-based controller to ensure perturbation rejection and robustness to delay. A multi-model reference governor strategy is included to prevent the actuator saturation and the consequent loss of control. The proposed methodology is illustrated on a single-axis satellite system equipped with reaction wheels.

1. Introduction

Dealing with perturbations is one of the major concerns when designing a satellite attitude control system. In this regard, particular attention is devoted to handle the propellant slosh and the flexible appendages dynamics. Liquid fuel represents a considerable share of the total mass of a satellite and its dynamics is an undeniable risk of performance degradation and in rare cases of mission loss, especially when fuel tanks are half empty [1]. Moreover, the spacecraft flexible appendages can induce structural oscillations imposing severe limitations on the achievable control system capabilities. While modelling and controlling the latter have been widely established, handling sloshing dynamics in microgravity remains a debated topic. Most widespread approaches employ passive solutions, such as baffles and bladders, to mitigate the low frequency propellant motion [2], [3]. Such solution has the advantage of not resorting to an accurate sloshing disturbance torque model, which is notably difficult to obtain in microgravity, but the price to pay is an increase of weight, cost and complexity of manufacturing. Alternatively, other approaches either smoothen the reference angular velocity or introduce time margins between aggressive manoeuvres so as to lower the propellant excitation [4], [5]. In both cases, despite the effective liquid motion handling, the resulting mission availability and the satellite agility are no longer exploited. Therefore, active control system solutions, capable of both precise attitude control and fuel slosh suppression, are of great interest and remain an active field of research.

From a control design perspective, a well established approach consists of modelling the sloshing disturbance torque via Equivalent Mechanical Models (EMM), [6], [7], [8], and to conceive *ad hoc* nonlinear and/or robust control frameworks to address the model uncertainties and inaccuracies [9], [10]. Their low complexity makes the existing EMMs particularly attractive, but a high adherence to the sloshing phenomenon, taking into account the nonlinear fluid behaviour and its dependence on the satellite speed and acceleration, is key to allow an improvement of both performance and robustness. In this context, novel slosh modeling approaches, including major contributions by ONERA and CNES in the framework of the joint research program COSOR (COmmande des Systèmes Orbitaux et Robotiques) [11], paved the way for investigating enhanced sloshing models and attitude control solutions. Inspired by EMMs and with the support of Computational Fluid Dynamics data, a nonlinear parameter-varying sloshing model has been proposed, [11]. Employing such a model, a robust observer-based attitude control has been developed in [12] and [13], where the sloshing torque is rewritten in a Linear Parameter-Varying (LPV) format to benefit of the hugely discussed control techniques developed for this class of systems. Consequently, the implementation of an LPV-based observer allowed to compensate the sloshing torque and to ensure the attitude requirements by means of a simple proportional-derivative control law. While the obtained results were very promising, handling the actuators saturations remained an unresolved issue. Concretely, to reject the sloshing disturbance, the commanded control action often leads the reaction wheels to reach their maximum angular speed and the resulting constant angular momentum makes the realized control torque drop to zero. In this scenario, while a rigid satellite results uncontrollable and swings around

DOI: 10.13009/EUCASS2022-4473

the reference attitude converging slowly, in presence of sloshing perturbations, the system can easily diverge. Recent contributions proposed in [14] enhanced such a control framework with a static Reference Governor (RG) to prevent actuator saturation while ensuring tracking performance specifications in presence of sloshing disturbances. Numerical simulations showed the effectiveness of this constraints handling strategy. Reference governors are add-on control schemes that filter the reference signal by solving at each time step a constrained linear optimization problem (LP) so as to enforce state and input constraints. Receiving as input the desired reference command $r(t)$ and the current state (estimated or measured) $x(t)$, the RG generates a modified reference $v(t)$ whenever propagating $r(t)$ may lead to constraints violation [15]. From the implementation point of view, employing RGs to handle the system constraints is particularly attractive to preserve the properties of an established controller. Unlike other approaches that aim at solving stabilization, tracking and constraints prevention, RGs are added on a predefined closed-loop system designed to ensure stability and performance and do not interact with its dynamics. In addition, one of the key advantages of RG with respect to other more complex constrained control strategies, such as Model Predictive Control, is the limited computational effort of the online implementation. This makes it extremely suitable for those applications that involve fast dynamics associated with limited computational capabilities, *i.e.*, automotive and aerospace systems.

Inspired by this approach, this paper proposes an RG-based robust controller to guarantee performance requirements in a more realistic space environment, notably characterized by the interaction of sloshing and flexible appendages modes. Differently from [14], where only one sloshing mode has been considered, the sloshing and the flexible perturbations are introduced as a superposition of three and four different modes respectively, so as to describe more accurately the disturbances acting on the system. In addition, the proposed robust observer is designed so as to allow for delay robustness with a low order control law. Finally, the RG scheme is adopted to enforce the actuator constraints and avoid the loss of control. Assuming a limited knowledge of the disturbance frequencies, an enhanced version of the RG, denoted as multi-model reference governor, is developed.

The paper is structured as follows: section 2 presents the open-loop satellite system together with the disturbance models considered, section 3 outlines the development of the robust observer to guarantee perturbation rejection. Next, the reference governor-based strategy is introduced in section 4 and the closed-loop system is augmented accordingly. In section 5, numerical simulations results underline the benefits of merging the robust observer with the RG. Final comments and future perspectives conclude the paper.

2. Open-loop system

The system consists of a satellite subject to sloshing perturbations and actuator saturations. The coupling between the three axes of the satellite is considered negligible with respect to the disturbance torques and therefore a single-axis control problem is investigated. The open-loop dynamics reads:

$$J\ddot{\theta} = \Gamma_{RW} + d(t) \tag{1}$$

where $J = 1000\ kg{\cdot}m^2$ and $\theta\ (rad)$ denote the inertia and the satellite attitude respectively. $d(t)\ (N{\cdot}m)$ embeds all the disturbances acting on the system, while the control input is the torque $\Gamma_{RW}\ (N{\cdot}m)$ realized by the reaction wheels. Their dynamics is modelled as a first order system with time constant $\tau = 0.5\ s$:

$$\frac{\Gamma_{RW}}{u} = \frac{1}{0.5s + 1} \tag{2}$$

The actuators are subject to symmetric saturations on the commanded input torque $u(t)$ and on the angular momentum H_{RW} ($u_{max} = 0.5\ N{\cdot}m$, $H_{max} = 10\ kg{\cdot}m^2{\cdot}s^{-1}$). Fig. 1 precises the open-loop dynamics. From a control design perspective, the angular momentum saturation has to be strictly avoided. *De facto*, when the maximum momentum is reached, the wheels can no longer be accelerated and cannot provide torque anymore. This is mathematically represented by a saturation placed between an integrator (which output coincides with the momentum) and a derivator (which output is zero when the input is saturated to a constant value).

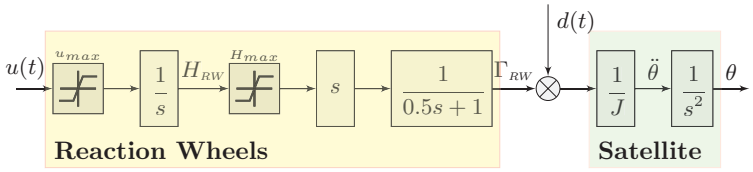

Figure 1: Satellite and actuators scheme

DOI: 10.13009/EUCASS2022-4473

2.1 Disturbance model

Satellite dynamics are typically subject to several kinds of disturbances. It is assumed that in addition to the sloshing and the flexible appendages disturbance torques, here denoted as Γ_S $(N{\cdot}m)$ and Γ_F $(N{\cdot}m)$ respectively, an additional unmodelled perturbation Γ_D $(N{\cdot}m)$ acts on the system. The latter is considered to be generated by a robotic arm aboard the satellite for on-orbiting servicing. Its dynamics is added in accordance to realistic robotic arm tasks from the PULSAR project (Prototype of an Ultra Large Structure Assembly Robot, [16]) adapted for the considered application, and starts acting after 400 s as illustrated in Fig. 2. Therefore, the total disturbance torque $d(t)$ can be expressed as:

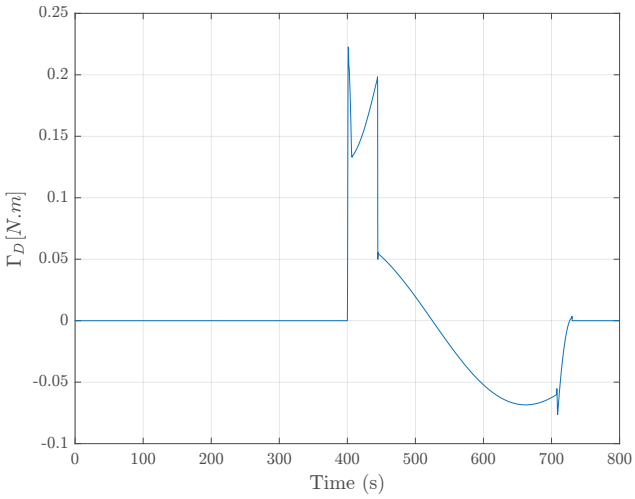

Figure 2: Robotic arm perturbation

$$d(t) = \Gamma_S + \Gamma_F + \Gamma_D \tag{3}$$

The sloshing and flexible appendages disturbances are added following the Cantilever Hybrid Model analogy proposed in [17]. The resulting torques are computed as the superposition of poorly damped and low-frequency linear time-invariant (LTI) second order dynamics, such as $\Gamma_{S,F} = \sum_i \Gamma_{S_i,F_i}$, that take as input the satellite angular acceleration $\ddot{\theta}$. Three sloshing and four flexible modes are considered. Therefore, the modes dynamics reads:

$$\Gamma_{S_i,F_i} = \frac{s^2}{s^2 + 2\xi_{S_i,F_i}\omega_{S_i,F_i}s + \omega^2_{S_i,F_i}} L_{S_i,F_i}\ddot{\theta} \tag{4}$$

where L_{S_i,F_i} are the modal contribution matrix components, ω_{S_i,F_i} the pulsations and ξ_{S_i,F_i} the damping ratios of the i^{th} flexible/slosh mode. According to experimental data from [11], these parameters are chosen as $L_{Si} \in [30, 50]$, $\omega_{Si} \in [0.1, 0.3]$, $\xi_{Si} \in [0.001, 0.03]$, $L_{Fi} \in [50, 300]$, $\omega_{Fi} \in [0.6, 10]$, $\xi_{Fi} \in [10^{-4}, 10^{-3}]$. The lower-bound of the flexible proper frequency range is deliberately set smaller than the standard values found in the literature in order to analyze potential interactions between the two phenomena. In addition, it is assumed that the fluid is initially at rest and that its mass variation is negligible during a single maneuver. This LTI representation allows for easily manipulating the slosh/flexible frequency characteristics so as to analyze the control law robustness against modeling uncertainties. Fig. 3 compares the frequency characteristics of the system with and without perturbations. At very low frequencies ($\omega \ll 0.1$) the full order dynamics coincide with those of the rigid body (double integrator). Conversely, at higher frequencies, significant differences appear with numerous resonant modes.

3. Robust controller design

In order to justify the need of a law specifically conceived to handle perturbations, preliminary simulations are performed with a proportional-derivative (PD) controller developed considering the rigid body configuration ($i.e.$, no perturbations acting on the system). The control law also includes a feedforward controller and simply reads:

$$u = K_p(\theta_r - \theta) + K_d(\dot{\theta}_r - \dot{\theta}) + J\ddot{\theta}_r \tag{5}$$

Given an attitude requirement in the form of a step signal θ_c, the reference profiles θ_r, $\dot{\theta}_r$ and $\ddot{\theta}_r$ are computed smoothing it down by means of a second order transfer function so as to get three feasible signals to track. The system states θ and

DOI: 10.13009/EUCASS2022-4473

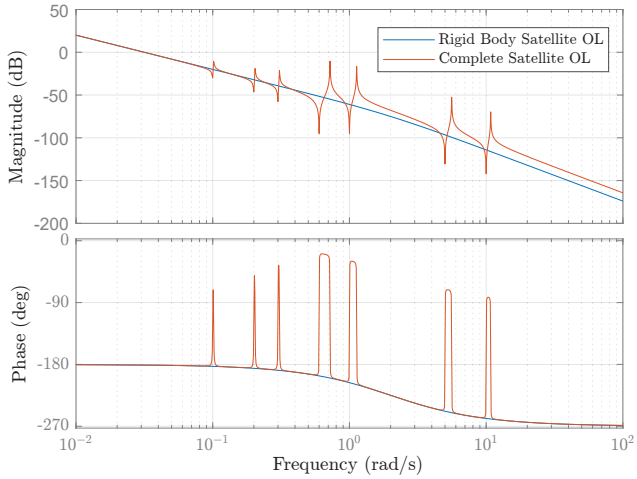

Figure 3: Open-loop analysis

$\dot{\theta}$ are assumed to be perfectly measured or estimated. The proportional and derivative gains $K_p = 2.4$ and $K_d = 69$ are computed by forcing the system closed-loop poles to correspond to those of the LTI second-order system described by a natural frequency $\omega = 0.1$ and a damping ratio $\xi = 0.7$. Fig. 4 illustrates the control architecture, where $PD = [K_p, K_d]$ and with K_c initially set to 0. Fig. 5 compares the attitude errors in the cases with and without perturbations for an

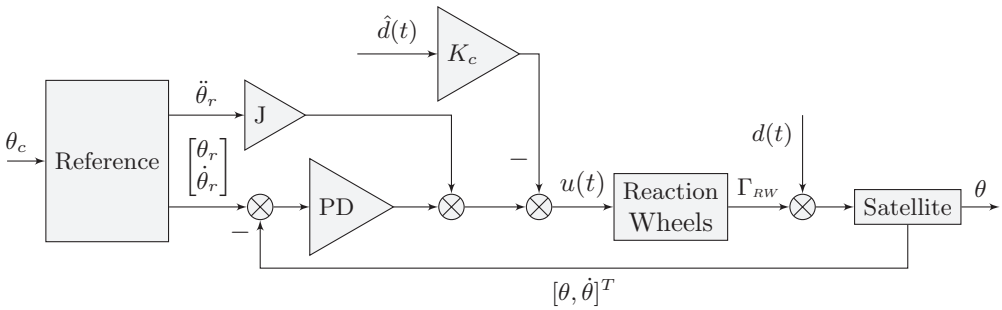

Figure 4: Preliminary controller implementation

input step $\theta_c = 0.2\ rad$. While an accurate tracking is ensured for the rigid body case, the simple PD law is not able to deal with the disturbances and the residual attitude error $(\theta_r - \theta)$ is around $10^{-3}\ rad$ and even higher after 400 s, when the robotic arm starts operating. With the intention of highlighting the effectiveness of a law aimed at handling disturbances, the results of the same PD controller enhanced with an observer-based disturbance compensation strategy is included in the plot. For this purpose, an ideal perfect (and unrealistic) observer is here considered setting $\hat{d}(t) = d(t)$ and $K_c = 1$ in the scheme of Fig. 4. As shown in Fig. 5, all perturbations are greatly modulated confirming the need for an advanced strategy for disturbances handling. Unfortunately, the great tracking performance of the observer-based strategy is accompanied by a severe decrease of gain, phase and delay margins. In particular, the latter is equal to $\tau_d = 0.15\ s$ and occurs at rather high frequencies ($11\ rad/s$), which suggests that the destabilization is induced by the flexible modes perturbation. Fig. 4 shows that the system diverges if an actuator delay of $\tau_d = 0.16\ s$ is introduced. For this reason, it is here proposed to design an H_∞-based controller so as to ensure perturbation rejection together with robustness to a reasonable delay.

3.1 H_∞ synthesis

By means of an H_∞-based strategy, it is aimed to design a dynamic controller $K(s)$ with a twofold purpose: minimize the attitude error in presence of disturbances and ensure a solid robustness to delay. $K(s)$ will receive three inputs: the integral of the attitude error, the attitude error and the angular velocity error. Hence, the resulting controller will present the same general structure of a proportional-integral-derivative (PID) law with dynamic gains K_I, K_P and K_D. Two exogenous inputs are considered: the reference attitude w_1 and the disturbance torque w_2. Finally, three exogenous outputs are used: the attitude error z_1, the integral of the attitude error z_2 and the commanded torque z_3. The scheme

DOI: 10.13009/EUCASS2022-4473

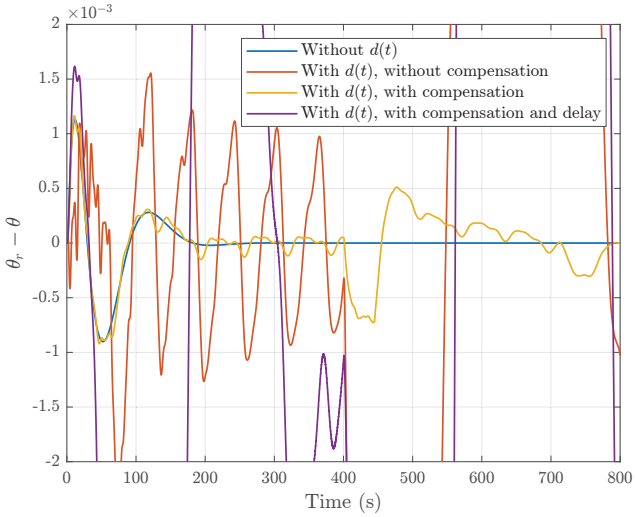

Figure 5: Attitude error with VS without disturbances, PD controller, $\theta_c = 0.2\ rad$

employed for the design of the controller is presented in Fig. 6, where $K(s)$ is placed between the output y_0 (dimension 3) and u_0 (dimension 1). The optimization problem to be solved reads:

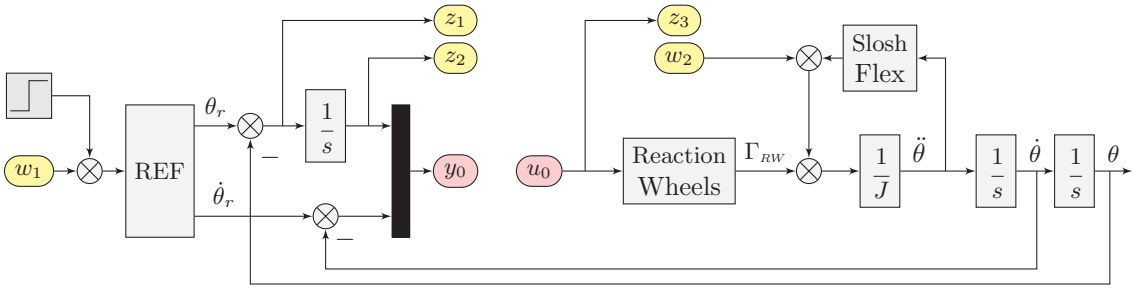

Figure 6: H_∞ synthesis

$$K(s) = arg \min_{K(s)} \{ \left\| T_{(w_1,w_2)\to z_1}(s) \right\|_\infty , \left\| T_{w_2\to z_2}(s) \right\|_\infty , \left\| W_D(s) \cdot T_{w_2\to z_3}(s) \right\|_\infty \} \tag{6}$$

The first transfer function $T_{(w_1,w_2)\to z_1}$ aims at penalizing the attitude error in presence of reference signals and perturbations at all frequencies. $T_{w_2\to z_2}$ is used to penalize the integral of the attitude error in presence of torque perturbations. This will enforce the integral action of the PID controller by minimizing the effect of perturbations at low frequencies. Finally, $T_{w_2\to z_3}$ is employed to deal with delay margin since it can be interpreted as the transfer seen by an additive uncertainty $\Delta(s)$ on the actuator $A(s)$:

$$A(s) \to A(s) + \Delta(s) \tag{7}$$

Supposing that the actuator is subject to a certain delay τ, then $\Delta(s)$ can be rewritten as:

$$\Delta(s) = (\exp^{-\tau s} - 1) A(s) \tag{8}$$

By determining a filter $W_D(s)$, such that:

$$\forall \omega \geq 0, \forall \tau \in [0, \tau_{max}], |W_D(j\omega)| \geq |(\exp^{-j\omega\tau} - 1) A(j\omega)| \tag{9}$$

then, by virtue of the small gain theorem, the controller $K(s)$ will robustly stabilize the closed-loop system in the presence of any delay smaller than τ_{max} if:

$$\left\| W_D(s) \cdot T_{w_2\to z_3}(s) \right\|_\infty \leq 1 \tag{10}$$

DOI: 10.13009/EUCASS2022-4473

$W_D(s)$ is found via a modal approach by setting $\tau_{max} = 0.4\ s$. Fig. 7 shows the actuator dynamics for all delays in the range of $\tau \in [0, \tau_{max}]$. The gain of the proposed filter verifying (9) is visualized by the black plot. Its transfer function reads:

$$W_D(s) = \frac{0.4125s}{1 + 0.55s} \tag{11}$$

$W_D(s)$ will be the only dynamic filter and will be placed on the output z_3, two constant weight functions are applied

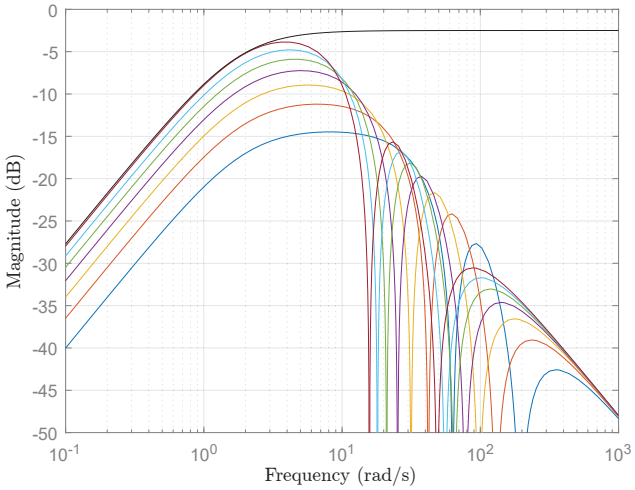

Figure 7: Approximations of $\Delta(s)$ such that $A(s) + \Delta(s) = \exp^{-\tau s} A(s)$ with $\tau \in [0, 0.4]$

on z_1 and z_2 ($W_{o1} = 50, W_{o2} = 5$). Finally, a constant filter $W_{i2} = 5$ is placed in input on w_2 so as to reinforce the perturbation rejection. The controller synthesis is initially performed by means of the standard convex optimization algorithm implemented in the routine `hinfsyn` of the MATLAB Robust Control Toolbox, [18], [19]. The obtained controller $K(s)$ is of order 21 due to the numerous flexible modes of the model. A strong perturbation rejection is ensured, together with a strong delay robustness ($\tau_d = 0.95\ s$). Fig. 8 illustrates the simulation results setting a delay of $0.4\ s$. The resulting attitude error remains in the order of $10^{-5}\ rad$ and is greatly bounded even when the robotic arm perturbation is introduced. The commanded torque saturation is slightly reached at the beginning of the simulation but results are not affected.

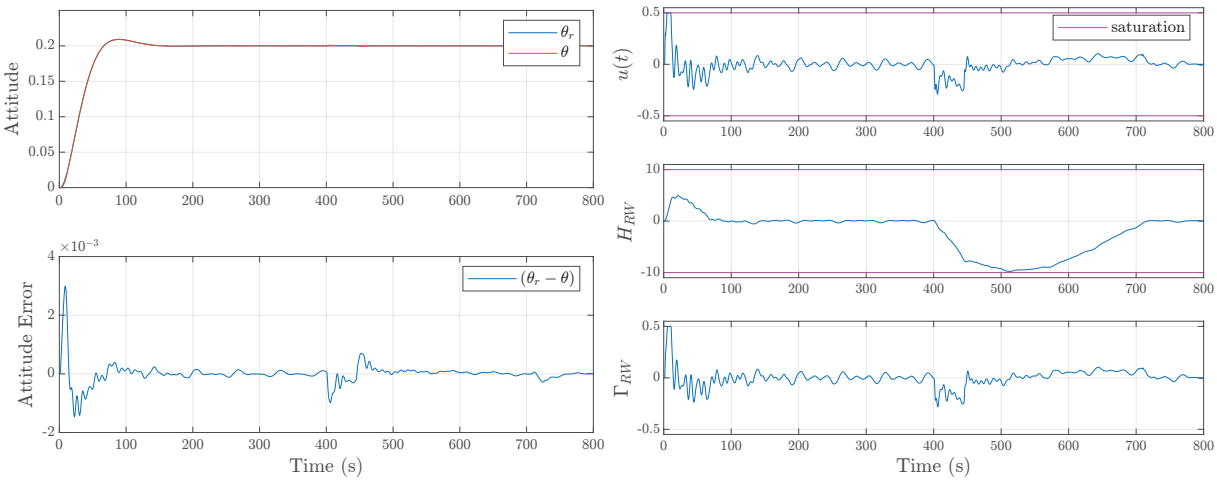

(a) (b)

Figure 8: Attitude tracking, H_∞-based controller order 21

With the intention of reducing the calculation workload, an advanced synthesis setting the order of the controller to 5 is realized using the MATLAB routine `systune`. In addition, a constraint on the upper bound of the gains is set to 1000 to limit the control effort. Finally, the controller poles are also constrained so as to regulate their dynamics at high frequency. The obtained delay robustness appears reduced to $\tau_d = 0.46\ s$, but still above the desired threshold

DOI: 10.13009/EUCASS2022-4473

$\tau_{max} = 0.4\ s$; the new gains $K_I(s)$, $K_P(s)$ and $K_D(s)$ are compared with the previous ones in Fig. 9. As shown, while $K_I(s)$ and $K_P(s)$ are reduced at all frequencies, $K_D(s)$ remains particularly high at low frequencies imposing a precise estimation of the angular velocity. Fig. 10 shows a little reduction of precision compared to the controller of order 21.

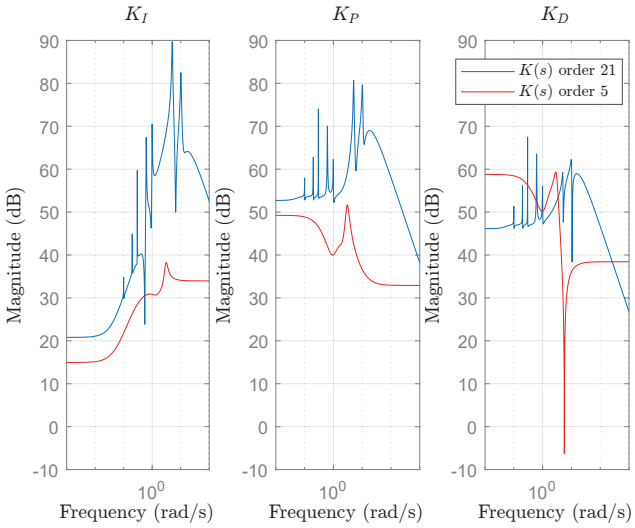

Figure 9: Gains controller order 21 VS order 5

While during the transient phase performance are comparable, at steady state the perturbation rejection results degraded and the attitude error is in the order of $10^{-4}\ rad$, suggesting that the choice of the most suitable controller among the two has to be driven by computational workload constraints. Hereinafter, results are shown for the controller of order 5. The control effort of the two controllers is comparable. For low amplitude step manoeuvres, the reaction wheels are far from saturation and performance are ensured.

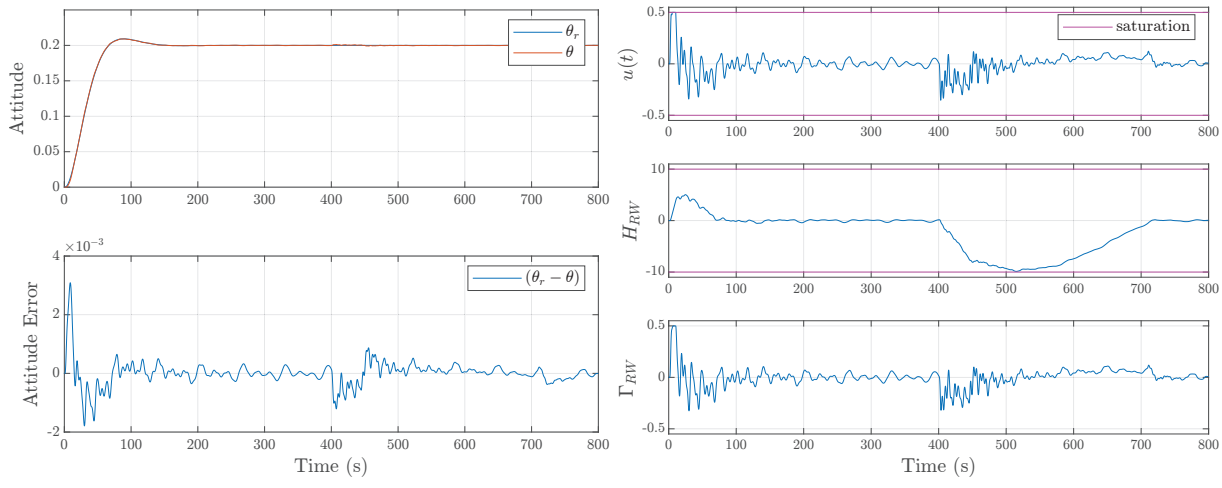

(a) (b)

Figure 10: Attitude tracking, H_∞-based controller order 5, $\theta_c = 0.2\ rad$

On the contrary, for larger demanded angles, the nonlinearities introduced by the actuator saturation lead to unstable dynamics. Fig. 11 presents results for a step manoeuvre of $\theta_c = 0.35\ rad$ for the controller of order 5. As it can be noticed, the commanded torque cannot be realized due to the actuator capabilities and saturations are inevitable. The maximum angular momentum is reached, the realized reaction wheels torque Γ_{RW} drops to zero, and the controller has no more authority on the attitude angle. In conclusion, all the benefits of the proposed solution are lost if the scheme is not augmented with a strategy to enforce the actuator constraints.

DOI: 10.13009/EUCASS2022-4473

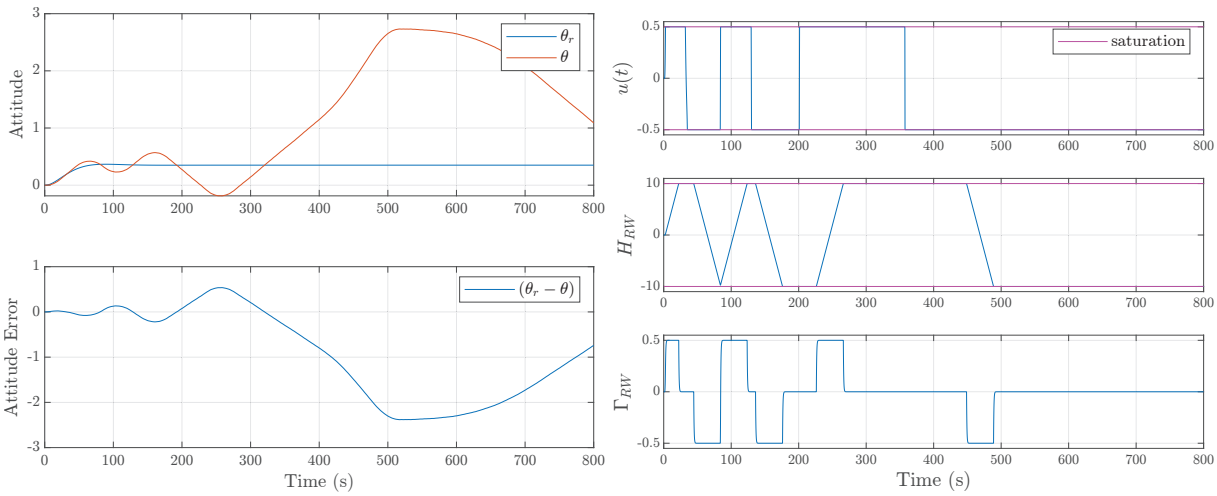

Figure 11: H_∞-based controller performance degraded by saturations, $\theta_c = 0.35\ rad$

4. Reference governor

Reference governors are add-on control blocks that act as a prefilter between an input reference signal and the closed-loop system. The RG-based control scheme is given in Fig. 12. Based on the current values of the input $r(t) \in \mathbb{R}^{q\times 1}$ and of the estimated state $\hat{x}(t) \in \mathbb{R}^{p\times 1}$, RG computes at each time step the best approximation $v(t) \in \mathbb{R}^{q\times 1}$ of the desired input $r(t)$ such that, applying a constant signal v along a predefined horizon N, input and state constraints are satisfied at each discrete time step $n \in N$. Merging all constraints in the output variable $y(t) \in \mathbb{R}^{r\times 1}$ and implementing RG in discrete time, then the maximal constraint admissible set O_∞ is defined as:

$$O_\infty = \{(v, \hat{x}) : \tilde{y}(n \mid v, \hat{x}) \in Y, \forall n \in N\} \tag{12}$$

where $\tilde{y}$ defines the predicted constrained variables, Y specifies the constraints set and $N \in \mathbb{R}_+$ is the time horizon on which the prediction is computed, usually chosen so as to reach steady state. For computational reasons and to guarantee the maximal admissible set to be finitely determined (see [20]), a tightened version of O_∞, namely $\tilde{O}_\infty$, is employed so that constraints are satisfied with a nonzero margin $\epsilon > 0$:

$$\tilde{O}_\infty = \{(v, \hat{x}) : \tilde{y}(n \mid v, \hat{x}) \in (1-\epsilon)Y, \forall n \in N\} \tag{13}$$

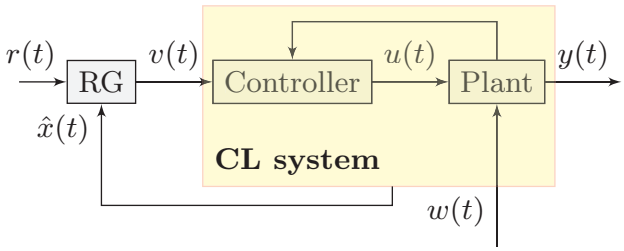

Figure 12: RG-based controller scheme

By solving a linear programming optimization problem, RG computes $v(t)$ so as to minimize the distance between the desired reference $r(t)$ and to enforce constraints assuming the signal v constant on the whole horizon N:

$$\begin{aligned} v(t) &= \arg\min_v (v - r(t)) \\ &\text{s.t.} (v, \hat{x}(t)) \in \tilde{O}_\infty \end{aligned} \tag{14}$$

By virtue of what was just stated, it is remarked that the modified reference computed at time $t-1$ remains feasible, but possibly sub-optimal, even at time t.

DOI: 10.13009/EUCASS2022-4473

4.1 Reference governor implementation

In the considered application, the RG is employed to prevent the actuator saturations and hence avoid the satellite control loss. Being the non-saturated closed-loop system linear-time invariant, a correspondent discrete-time prediction model can be expressed as:

$$\begin{aligned} x_{n+1} &= Ax_n + Br_{n=1} \\ y_n &= Cx_n + Dr_{n=1} \end{aligned} \tag{15}$$

with

$$r_{n=1} = r(t) = \theta_c(t) \tag{16}$$

where x_n is the state vector such that $x_{n=1} = \hat{x}(t)$, $r_{n=1}$ is the input vector corresponding to the commanded attitude θ_c at time t, and y_n is the output vector gathering the states subject to constraints. The matrices $A \in \mathbb{R}^{p\times p}$, $B \in \mathbb{R}^{p\times q}$, $C \in \mathbb{R}^{r\times p}$ and $D \in \mathbb{R}^{r\times q}$ are obtained through the discretization of the stable closed-loop system discussed in section 3 using a sampling time δ_T. It is assumed that $\hat{x}(t)$ is perfectly measured or estimated, and that the external disturbances $w(t)$ of Fig: 12 are modelled in accordance to section 2.1 and included in the system matrices. Since the constrained states u and H_{RW} and their propagation are obtained as a linear combination of the estimated state $\hat{x}(t)$ and of the modified reference signal v, then the optimization problem can be written as an LP problem:

$$v(t) = \arg\min_{v} \mid v - r(t) \mid \quad \text{s.t.} \quad A_S \begin{bmatrix} \hat{x}(t) \\ v \end{bmatrix} \leq b_S \tag{17}$$

where the matrices $A_S \in \mathbb{R}^{2Nr\times(p+q)}$ and $b_S \in \mathbb{R}^{2Nr\times 1}$ are computed offline so as to enforce constraints by simply propagating the recurrent equations (15) on the horizon N. A_S multiplied by $[\hat{x}(t) \quad v]^T$ predicts the constrained states $\tilde{y}_n = [u_n \quad H_{RW_n}]$, as well as their opposite $-\tilde{y}_n$, for $n = 1, ..., N$. By doing so, A_S accounts for both upper and lower bounds constraints ($i.e.$, $-y_{max} \leq \tilde{y}_n \leq y_{max}$ with $y_{max} = [u_{max} \quad H_{max}]^T$), through an inequality of the kind $[\tilde{y}_{n,...,N} \quad -\tilde{y}_{n,...,N}]^T \leq b_S$, where b_S gathers the constraints bounds. The resulting matrices read:

$$A_S = \begin{bmatrix} CA^n & C\sum_{j=1}^{n} A^{j-1}B + D \\ \vdots & \vdots \\ CA^N & C\sum_{j=1}^{N} A^{j-1}B + D \\ -CA^n & -(C\sum_{j=1}^{n} A^{j-1}B + D) \\ \vdots & \vdots \\ -CA^N & -(C\sum_{j=1}^{N} A^{j-1}B + D) \end{bmatrix}, \qquad b_S = [(y_{max})_{\times 2N}]^T \tag{18}$$

From this preliminary formulation, a more efficient implementation is proposed by exploiting the fact that the modified reference computed at time $t-1$ remains feasible, but eventually sub-optimal, even at time t. Assuming that the time horizon has been chosen large enough to ensure that a steady state is reached and that the optimization problem has been solved at time $t-1$, then the modified reference $v(t-1)$ is a feasible solution of the optimization problem even at the time t as it verifies:

$$A_S \begin{bmatrix} \hat{x}(t) \\ v(t-1) \end{bmatrix} \leq b_S \tag{19}$$

Then, the modified reference $v(t)$ can be expressed as a function of the current value $r(t)$ and of the previous modified one $v(t-1)$ by introducing a parameter $k \in [0\ 1]$:

$$v(t) = v(t-1) + k(r(t) - v(t-1)) \tag{20}$$

with

$$k = \max_{k\in[0\ 1]} k \quad \text{s.t.} \quad A_S \begin{bmatrix} \hat{x}(t) \\ v(t-1) + k(r(t) - v(t-1)) \end{bmatrix} \leq b_S \tag{21}$$

The optimization problem has been redefined. The optimization variable k is simply constrained to be searched in the range $[0\ 1]$, allowing for more computational efficiency, and the optimization problem becomes a maximization problem. If $k = 0$, then the previous reference is employed ($v(t) = v(t-1)$); on the contrary, if $k = 1$, then no saturation is predicted and $v(t) = r(t)$. Finally, (21) can be reformulated as:

$$k = \max_{k\in[0\ 1]} k \quad \text{s.t.} \quad \alpha_k k \leq \beta_k \tag{22}$$

DOI: 10.13009/EUCASS2022-4473

with

$$\begin{cases} \alpha_k = A_{S_v}(r(t) - v(t-1)) \\ \beta_k = b_S - A_{S_v} v(t-1) - A_{S_x}\hat{x}(t) \end{cases} \tag{23}$$

where the A_{S_v} and A_{S_x} are the two vertical blocks of matrix A_S, in (18). The resolution of (22) is straightforward and very well suited for online implementation. It does not require any advanced linear or quadratic programming techniques. Let us denote α_{k_j} and β_{k_j} the j^{th} elements of α_k and β_k respectively, then, by observing that $\beta_{k_j} \geq 0$, it can be stated that:

$$k = \min\{k_1, ..., k_{2Nr}\} \tag{24}$$

with

$$\begin{cases} \alpha_{k_j} \leq 0 \implies k_j = 1 \\ \alpha_{k_j} > 0 \implies k_j = \min\{1, \frac{\beta_{k_j}}{\alpha_{k_j}}\}. \end{cases} \tag{25}$$

Multi-model reference governor

The RG implementation is made considering both fuel sloshing and flexible appendages perturbations precisely known, which is inevitably not the case in reality, and uncertainties have to be accounted. To include robustness properties while remaining the least conservative possible, the RG scheme is reformulated with a multi-model strategy. The single system (15) is replaced by a family of m models that take into account possible variations of the closed-loop system matrices.

$$\begin{aligned} x_{n+1} &= A_i x_n + B_i r_{n=1} \\ y_n &= C_i x_n + D_i r_{n=1}, \quad i = 1, ..., m \end{aligned} \tag{26}$$

The matrices A_{S_v}, A_{S_x} and b_S are updated accordingly so as to incorporate all constraints imposed by the m models. Despite the number of constraints is increased by a multiplicative factor m, the LP problem remains computationally cheap thanks to the offline implementation of A_{S_v}, A_{S_x} and b_S. Referring to the sloshing and flexible appendages model (4), several values of natural frequency ω_{S_i,F_i} are accounted so as to reduce the assumed knowledge of the perturbation model and enhance the robustness of the controller. To this purpose, multiplicative uncertainties are introduced on the nominal pulsations of the slosh and flexible modes:

$$\omega_{S_i} = (1 + \delta_{S_i})\omega_{S_{0_i}} \tag{27}$$

$$\omega_{F_i} = (1 + \delta_{F_i})\omega_{F_{0_i}} \tag{28}$$

where $\omega_{S_{0_i}}$ and ω_{F0_i} are the nominal values of frequencies employed in the previous simulations: $\omega_{S_{0_i}} = [0.1, 0.2, 0.3]$ and $\omega_{F_{0_i}} = [0.6, 1, 5, 10]$. A first implementation is made considering $\delta_{S_i,F_i} = \{-0.2, 0.2\}$. Hence, four limit configurations of perturbations corresponding to the vertex of the square space of Fig. 13 are obtained in addition to the nominal one. Satisfying the set of constraints describing the five configurations does not allow to infer anything regarding the other couples of frequencies lying within the four vertex. An interesting approach to overcome this limit consists in increasing the mesh density. Again, all couples of frequencies between points might lead the actuators to reach saturation, but considering a very dense mesh, the saturation period is ensured to be strongly reduced and the consequent loss of control avoided. In terms of computational cost, the number of constraints would be definitely increased, but the offline computation of the matrices A_{S_v}, A_{S_x} and b_S would still make the optimization problem fairly acceptable in terms of time consumption. In addition, given the numerous constraints that would be obtained, an intriguing further implementation could include an extra offline treatment of the matrices so as to delete all redundant or useless constraints and limit even more the computational cost. Fig. 14 illustrates the idea behind the approach. For illustrative purposes, a simple 2D space described by the states x_1 and x_2 is considered. Assuming the m^{th} model associated to the m^{th} constraint c_m, then the polytope within which the two states can lie is described by a set of l linear constraints, with $l \leq m$. As shown in the figure, c_6 does not contribute to the definition of the polytope and can be discarded. Applying this idea on a large bunch of points in a multi dimensional space can significantly reduce the number of constraints of the optimization problem and therefore the computational cost.

5. Numerical Simulations and Results Analysis

Numerical simulations and results demonstrate the benefits of including the reference governor scheme. An extensive validation campaign has been performed with the scope of testing the controller perturbation robustness in several nominal and off-nominal conditions. For the sake of space, only the most relevant are reported in the article .

DOI: 10.13009/EUCASS2022-4473

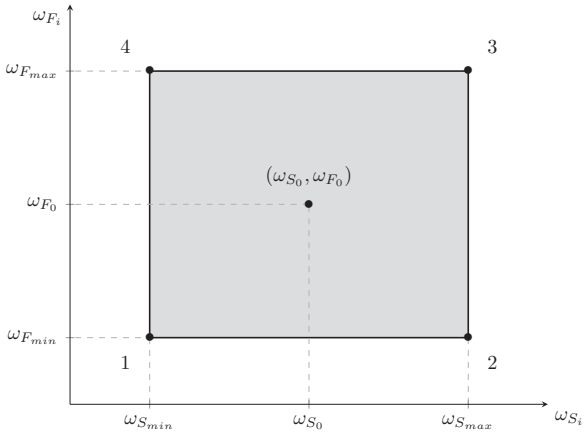

Figure 13: Multi-model reference governor implementation strategy

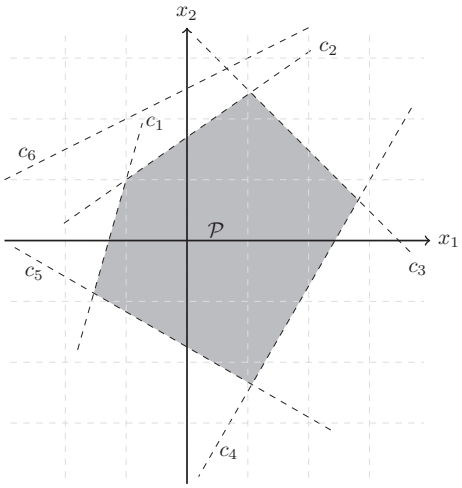

Figure 14: Constraints polytope

The same scenario of Fig. 11 is considered so as to compare results with and without RG. A step manoeuvre of $\theta_c = 0.35\ rad$ is realized with the controller of order 5, the nominal slosh and flexible appendages frequencies and a time delay of $\tau_d = 0.4\ s$. Fig. 15 clearly proves the benefits of the RG strategy: from a complete loss of control to precise tracking and saturation prevention. The last subplot on the left shows how the reference $r(t)$ is modified into $v(t)$. Thanks to the RG block, larger angles can be tracked without constraints violation and the system safety is ensured. This standard RG approach considers the disturbances perfectly known and does not account for possible perturbation model uncertainties. To overcome this limit the multi-model strategy is implemented.

Fig. 16 compares results with and without the multi-model configuration for a step manoeuvre of $\theta_c = 0.5rad$ realized with the controller of order 5 and time delay $\tau_d = 0.4\ s$. The sloshing and flexible appendages frequencies are modified from the nominal value and set to the upper bound considered, *i.e.*, $\omega_{S_i,F_i} = (1 + \delta_{S_i,F_i})\omega_{S_{0_i},F_{0_i}}$ with $\delta_{S_i,F_i} = 0.2$ (analogous results are obtained for the three other combinations of frequencies). The simulation reveals that the saturation prevention of the standard RG did not function and the upper bounds of the reaction wheels torque and angular momentum are reached. From the plot of the attitude, it is evident that the standard RG formulation cannot guarantee the safety of the system. On the contrary, the multi-model approach firmly enforces constraints and therefore performance. As expected, the last subplot on the left shows that the standard RG reaches the desired reference $r(t)$ before the multi-model scheme. This result derives from the larger set of constraints considered in the multi-model approach. The standard RG cannot prevent saturation for any configuration but the nominal one, and therefore 'permits' the use of $r(t)$ before the multi-model, leading to overcome the actuator limits.

Finally, Fig. 17 proposes results for all the five combinations of frequencies considered. As it can be noticed,

DOI: 10.13009/EUCASS2022-4473

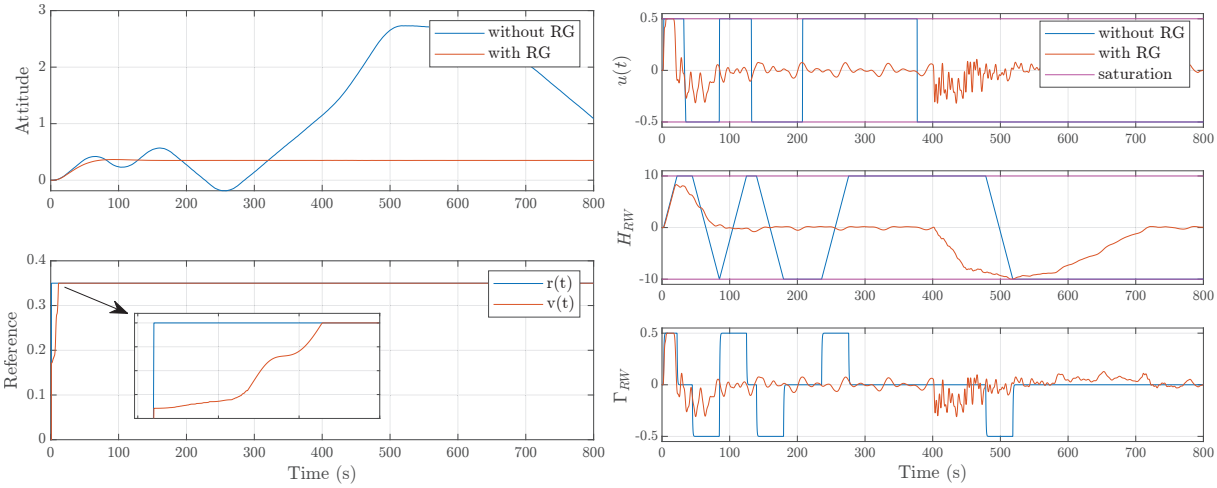

(a) (b)

Figure 15: without VS with RG, controller order 5, $\theta_c = 0.35\ rad$, $\tau_d = 0.4\ s$

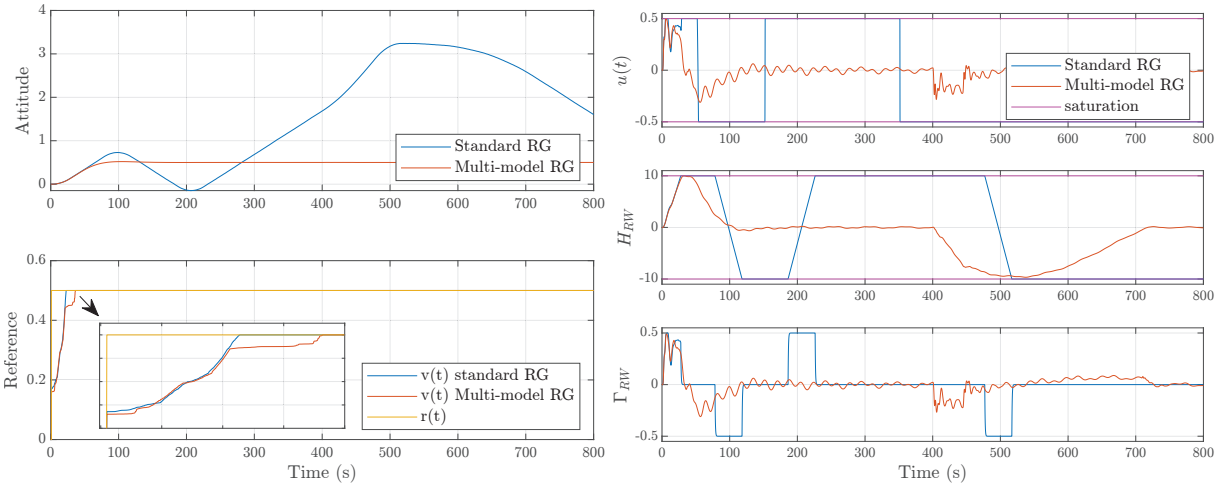

(a) (b)

Figure 16: Standard RG VS multi-model RG, controller order 5, $\theta_c = 0.5\ rad$, $\tau_d = 0.4\ s$, $\omega_{S_i,F_i} = 1.2\omega_{S_{0_i},F_{0_i}}$

saturation is well prevented in all cases. Additional simulations have been run implementing a multi-model reference governor that does not include the constraints relative to the original system (where $\omega_{S_i,F_i} = \omega_{S_{0_i},F_{0_i}}$). Results showed that if the perturbations are added considering the original pulsations, then saturation cannot be prevented and the system diverges, suggesting that an extensive study of the optimal mesh density is crucial.

6. Conclusions

Based on recent sloshing perturbation modeling, a novel solution for satellite attitude control has been developed. The approach consists of an H_∞-based synthesis to handle multiple perturbations, including sloshing and flexible appendages dynamics, and to ensure robustness to actuator delay. The control framework is augmented with a multi-model reference governor scheme to enforce actuators constraints and prevent the loss of control of the system. Robustness to perturbation variations is also ensured thanks to the multi-model formulation. A possible interaction of propellant slosh and flexible appendages dynamics was also investigated and the implemented controller allowed an effective rejection and a precise tracking. The campaign validation performed on a single-axis satellite verified the effectiveness of the proposed strategy. Future works will include major uncertainties in the disturbance models, *i.e.*, on the damping ratio, so as to investigate widely the robustness of the approach. An extensive study on the required mesh density of the uncertainties space is also foreseen, together with a possible constraints elimination strategy. In addition, aiming at reducing the static

DOI: 10.13009/EUCASS2022-4473

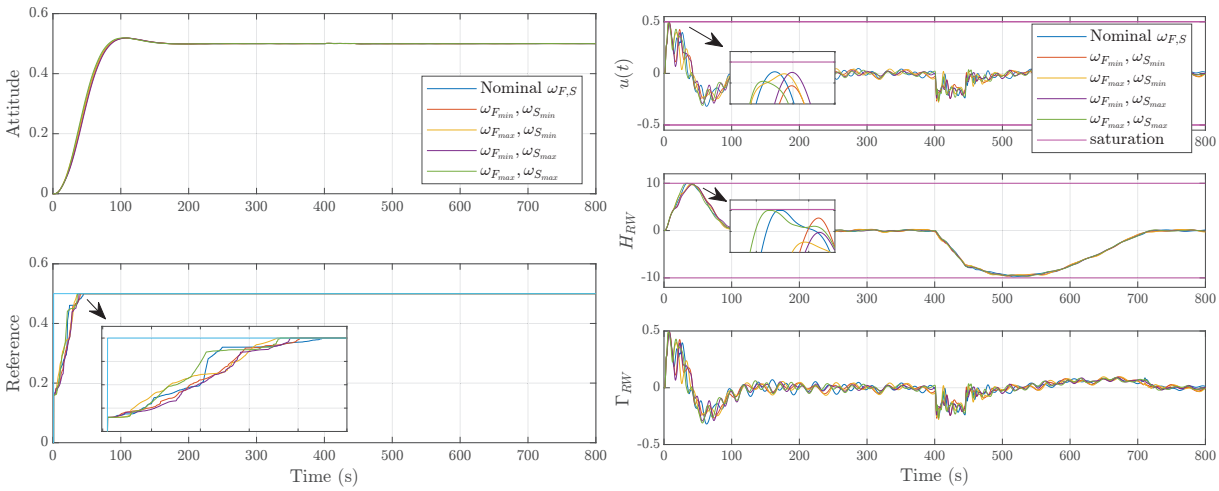

(a) (b)

Figure 17: Multi-model RG, controller order 5, $\theta_c = 0.5\ rad$, $\tau_d = 0.4\ s$, ω_{S_i,F_i} variations

reference governor conservatism, the extended command governor formulation will be considered, see [21]. This strategy includes fictitious dynamics to potentially provide a larger constrained domain of attraction and faster response at the price of increased computational complexity. Finally, a completely different approach to handle unmodelled disturbances based on adaptive control laws will be taken into account. In this case, the nonlinearities arising from the adaptive nature of the controller represent a great challenge when implementing a reference governor and will be investigated in the near future.

References

[1] E. J. Hoffman, W. Ebert, M. Femiano, H. Freeman, C. Gay, C. Jones, P. Luers, and J. Palmer. The near rendezvous burn anomaly of december 1998. *Applied Physics Laboratory, Johns Hopkins University, Tech. Rep*, 1999.

[2] F. T. Dodge. Engineering study of flexible baffles for slosh suppression (nasa cr-1880). *Tech. rep.*, 1971.

[3] W. Tam, K. Dommer, S. Wiley, L. Mosher, and D. Persons. Design and manufacture of the messenger propellant tank assembly. *38th AIAA/ASME/SAE/ASEE Joint Propulsion Conference & Exhibit*, 2002.

[4] X. Liu, X. Xin, and Z. Li. Near minimum-time feedback attitude control with multiple saturation constraints for agile satellites. *Chinese Journal of Aeronautics*, 2016.

[5] Y. Somov, S. Butyrin, S. Somov, and C. Hajiyev. Attitude guidance, navigation and control of land-survey mini-satellites. *IFAC OnLine, 48(9):222–227*, 2015.

[6] L. Mazzini. Flexible spacecraft dynamics, control and guidance. *Springer*, 2015.

[7] F.T. Dodge. The new "dynamic behavior of liquids in moving containers". *Southwest Research Inst. San Antonio, TX*, 2000.

[8] P. Sopasakis, D. Bernardini, H. Strauch, S. Bennani, and A. Bemporad. Sloshing-aware attitude control of impulsively actuated spacecraft. *European Control Conference*, 2015.

[9] M. Reyhanoglu and J.R. Hervas. Nonlinear dynamics and control of space vehicles with multiple fuel slosh modes. *Control Engineering Practice*, 2012.

[10] L.C.G. de Souza and A.G. de Souza. Satellite attitude control system design considering the fuel slosh dynamics. *Shock and Vibration*, 2014.

[11] A. Bourdelle, L. Burlion, J.-M. Biannic, H. Evain, S. Moreno, C. Pittet, A. Dalmon, S. Tanguy, and T. Ahmed-Ali. Towards new controller design oriented models of propellant sloshing in observation spacecraft. *AIAA SciTech 2019 Forum*.

DOI: 10.13009/EUCASS2022-4473

[12] J.-M. Biannic, A. Bourdelle, H. Evain, S. Moreno, and L. Burlion. On robust LPV-based observation of fuel slosh dynamics for attitude control design. *IFAC-PapersOnLine*, 52(28):170 – 175, 2019. 3rd IFAC Workshop on Linear Parameter Varying Systems LPVS 2019.

[13] A. Bourdelle, J.-M. Biannic, H. Evain, S. Moreno, C. Pittet, and L. Burlion. Propellant sloshing torque h_∞-based observer design for enhanced attitude control. *IFAC-PapersOnLine*, 52(12):286–291, 2019.

[14] A. Bourdelle, J.-M. Biannic, H. Evain, C. Pittet, S. Moreno, and L. Burlion. Modeling and control of propellant slosh dynamics in observation spacecraft with actuator saturations. *EUCASS*, 2019.

[15] E. Garone, S. Di Cairano, and I. Kolmanovsky. Reference and command governors for systems with constraints: A survey on theory and applications. *Automatica*, 2016.

[16] C. Ampatzis, S. Moreno, M. Delpech, J. Rodriguez, D. Nolke, D. Jones, and G. Visentin. H2020 pulsar d4.1 - d11.1b - technology review. *Technical Report*, 2019.

[17] J.-P. Chretien and C. Manceaux-Cumer. Minimal lft form of a spacecraft built up from two bodies. *AIAA Guidance, Navigation, and Control Conference and Exhibit*, 2001.

[18] P. Apkarian and D. Noll. Nonsmooth H_∞ synthesis. *IEEE Transactions on Automatic Control 51 (1), 71-86*, 2006.

[19] G. Balas, R. Chiang, A. Packard, and M. Safonov. Matlab robust control toolbox™, user's guide. *MathWorks*, 2015.

[20] Elmer G. Gilbert and Kok Tin Tan. Linear systems with state and control constraints: The theory and application of maximal output admissible sets. *IEEE Transactions on Automatic Control*, 36(9):1008 – 1020, 1991.

[21] L. Burlion and I. Kolmanovsky. Aircraft vision-based landing using robust extended command governors. *IFAC-PapersOnLine 53 (2), 14716-14723*, 2020.